IEEE Photonics Journal
An IEEE Photonics Society Publication

Propagation Losses of Slotted Photonic Crystal Waveguides

Volume 4, Number 5, October 2012

A. Di Falco
M. Massari
M. G. Scullion
S. A. Schulz
F. Romanato
T. F. Krauss

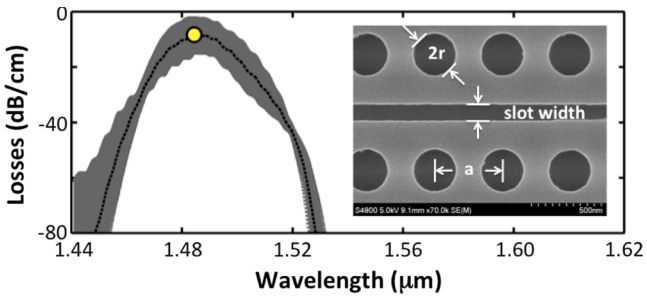

DOI: 10.1109/JPHOT.2012.2211342
1943-0655/$31.00 ©2012 IEEE

Propagation Losses of Slotted Photonic Crystal Waveguides

A. Di Falco,[1] M. Massari,[2] M. G. Scullion,[1] S. A. Schulz,[1] F. Romanato,[2] and T. F. Krauss[1]

[1]School of Physics and Astronomy, University of St Andrews, KY16 9SS Fife, U.K.
[2]LANN Laboratory for Nanofabrication of Nanodevices, 35127 Padova, Italy

DOI: 10.1109/JPHOT.2012.2211342
1943-0655/$31.00 ©2012 IEEE

Manuscript received June 27, 2012; revised July 27, 2012; accepted July 28, 2012. Date of publication August 2, 2012; date of current version August 15, 2012. The work of A. Di Falco was supported by an EPSRC Career Acceleration Fellowship (EP/I004602/1). Corresponding author: A. Di Falco (e-mail: adf10@st-andrews.ac.uk).

Abstract: We have fabricated and characterized a set of slotted photonic crystal (SPhC) waveguides in silicon-on-insulator (SOI) with a length of up to 300 μm and slot widths ranging between 115 and 145 nm. We observe an upper limit for the loss of 11 dB/cm.

Index Terms: Photonic materials and engineered photonic structures, engineered photonic nanostructures, waveguides, sensors, waveguide devices.

1. Introduction

Slotted photonic crystal (SPhC) waveguides provide control over the dispersion of light in air, both in the temporal and the spatial domain [1], [2]. They inherit this peculiarity from their geometry that combines two types of confining mechanisms, namely, guiding by a slot [3] and by a photonic crystal (PhC) lattice [4]. The PhC achieves guiding by resonant Bragg scattering, which also offers the ability to slow down light [5]. Slow light is one of the great advantages of PhC waveguides, as it enables large-bandwidth enhanced light–matter interactions, thus allowing a significant reduction in the length of the devices exploiting it. Additionally, cavities with high quality factor [6], [7] can be engineered through defects in the PhC periodic structure, providing another strong temporal confinement mechanism. The slot waveguide [3] geometry has enjoyed considerable success since it was introduced into integrated optics in 2004 due to the high degree of spatial light confinement it offers. Here, light is confined in a narrow slot region with low refractive index etched into a high refractive index medium, as a result of the sharp discontinuities in the optical field at each wall. Such behavior has since led to the use of the slot geometry for nonlinear enhancement [8], sensors [9], modulators [10], and the study of quantum effects [11]. SPhC devices bring together the advantages offered by both structures, and they have been used for chemical [12], [13] and bio-sensors [14] as well as for modulators [15]–[17]. For practical applications, both the benefits and the disadvantages of the technology have to be assessed, the key issues being coupling and propagation losses. Coupling losses have been thoroughly studied in SPhC devices, and different mechanisms have been suggested for their reduction, such as a multimode interference structure [18] or a tapered interface [17]. In Scullion *et al.* [19], we have introduced a coupler based on resonant defects and shown both high insertion efficiency (1.5-dB loss per interface) and large bandwidth (78 nm, centered at 1550 nm). Regarding propagation losses, these have been carefully addressed in both the slot waveguide [20]–[22] and the PhC case (see, e.g., O'Faolain *et al.* [23]), yet very little is known about the combined SPhC system. Here, we have addressed the issue by fabricating several SPhCs of different length

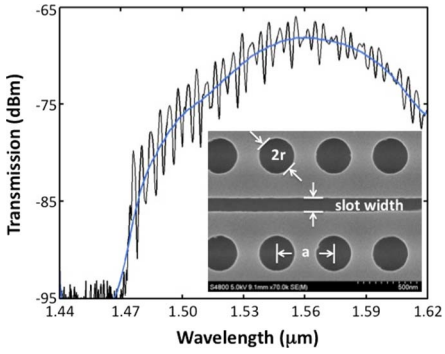

Fig. 1. Transmission curve in dBm for a typical SPhC waveguide, before and after filtering out the Fabry–Perot fringes that arise from interface reflections. The inset shows a SEM picture of the corresponding device.

and slot width. By using the cut-back method, we show how these losses depend on the slot width. With careful design, we find that these losses can be comparable to that of a standard channel slot waveguide, being of order of 10 dB/cm or better, and thus comparable to that of a standard PhC waveguide in the fast regime.

2. Fabrication and Measurements

The devices are made in silicon-on-insulator (SOI) substrates consisting of a 220-nm silicon layer on top of a 2-μm-thick SiO_2 buried oxide layer. Following standard cleaning procedure, the sample was coated with a 350-nm-thick layer of ZEP-520A electron beam resist and baked on a hot plate for 10 min at 180 °C. The electron beam exposure was performed at LaNN (Laboratory for Nanofabrication of Nanodevices, Padova, Italy) using a JEOL JBX-6300FS in high-resolution mode with an accelerating voltage of 100 kV, a writing current of 100 pA, and a beam diameter of 2 nm. The field size was 62.5 mm with estimated stitching errors of $+/-8$ nm. We wrote a range of devices with doses varying from 250 to 350 μC/cm^2. After exposure, samples were developed for 45 s in Xylene at room temperature and the pattern etched with a balanced blend of SF_6 and CHF_3 in a reactive ion etching system for 2 min at 20 W. An SEM picture of a typical sample is shown in the inset in Fig. 1, highlighting the relevant geometrical features. Choosing a lattice constant of $a = 490$ nm, a hole radius around $r \simeq 0.3a$, and a slot width in the interval (0.2a–0.3a, i.e., 100–150 nm) defines a SPhC waveguide with a bandgap in the C+L band, for TE polarization, with respect to the plane of periodicity. Fig. 1 shows the typical transmission spectrum, and we note considerable Fabry–Perot fringes arising from the interface between the slot waveguide and the (non-slotted) access waveguide. With careful design of the PhC interface (not used here), it is possible to eliminate this impedance mismatch, as we have shown previously [19]. Here, we focus on the propagation losses and note that the Fabry–Perot fringes can easily be filtered out numerically. In particular, we used a moving average technique, substituting each point with the average of the values within a centered window of 10-nm spectral width. For the characterization, we used a collimated and polarized white light supercontinuum source (Koheras compact) and end-fire coupling. Light was focused on the input facet with an aspheric lens (60X), and the output was collimated with a 40X aspheric lens. The signal was then focused onto a fiber beam splitter, delivering it to a photodetector (for alignment purposes) and an ANDO optical spectrum analyzer.

3. Experimental Results

To characterize the propagation losses, we fabricated SPhC waveguides with four different lengths (50, 100, 200, and 300 μm), for every different slot width. The relative filtered spectra are shown in Fig. 2, on a logarithmic scale. All the curves are normalized to the average transmissions of four different channel waveguides with 3-μm width, fabricated on the same chip along the SPhC waveguides. This normalization takes into account the coupling and propagation losses in the

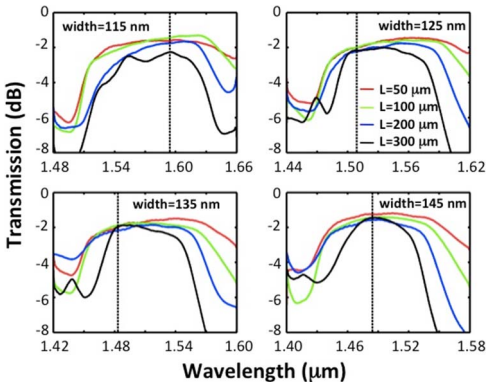

Fig. 2. Transmission curve in dB for different slot widths and lengths. In each panel, the dashed lines highlight the wavelength of minimum losses. The legend of the top right panel is valid for all slot widths.

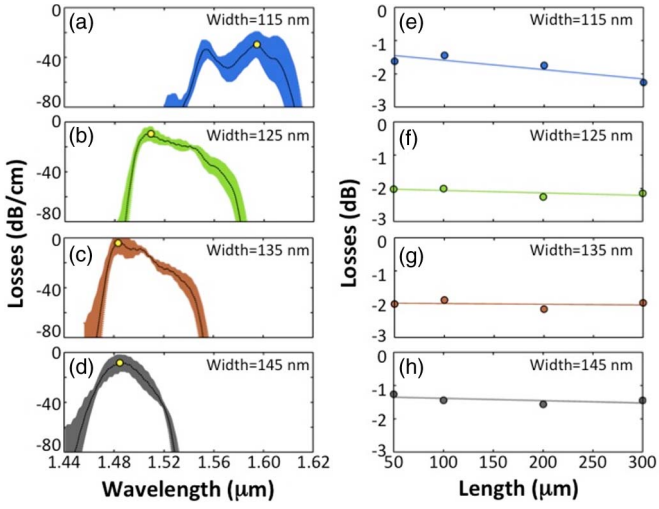

Fig. 3. (a)–(d) Losses in dB/cm versus wavelength for different slot widths. The shaded areas describe the standard deviation. (e)–(h) Losses versus waveguide length at the wavelength highlighted in panels (a)–(d). The continuous lines correspond to the linear best fit.

access waveguides. Every curve clearly shows low transmission on both the short- and the long-wavelength side; on the short-wavelength side, this is caused by the cutoff as the dispersion curve of the SPhC waveguide approaches the band edge [2], while on the long-wavelength side, the low transmission is due radiation losses as the dispersion curve crosses the light line. For longer waveguides, both mechanisms are clearly enhanced. The loss figure was extracted from the curves in Fig. 2. The cumulative result is collected in Fig. 3, in panels (a)–(d), which show the loss figure in dB/cm for four different slot widths as a function of wavelength. To obtain these curves, for a given slot width and for every wavelength, we plotted the normalized transmission versus waveguide length and calculated the best linear fit, resulting in a loss figure in dB/cm. Fig. 3(e)–(h) shows the measurements and linear fit corresponding to the wavelengths at which the minimum losses occur and are highlighted with circles in Fig. 3(a)–(d). These specific wavelengths correspond to the dashed lines in Fig. 2. To further clarify, the slope of the linear fit, shown, e.g., in panels (e)–(h), gives the loss figure in dB/cm, shown in panels (a)–(d) for every wavelength. The shaded areas of panels (a)–(d) describe the error estimates calculated from the least mean square fit, for each wavelength.

Table 1 summarizes the best loss figure for each slot width. The best performance is obtained for a slot width of 135 nm [see Fig. 3(c)], where we note $4 +/- 7$ dB/cm, i.e., an upper limit of 11 dB/cm.

TABLE 1

Slot width and best loss value

Slot width	Loss
115 nm	-29 ± 10 dB/cm
125 nm	-9 ± 5 dB/cm
135 nm	-4 ± 7 dB/cm
145 nm	-8 ± 6 dB/cm

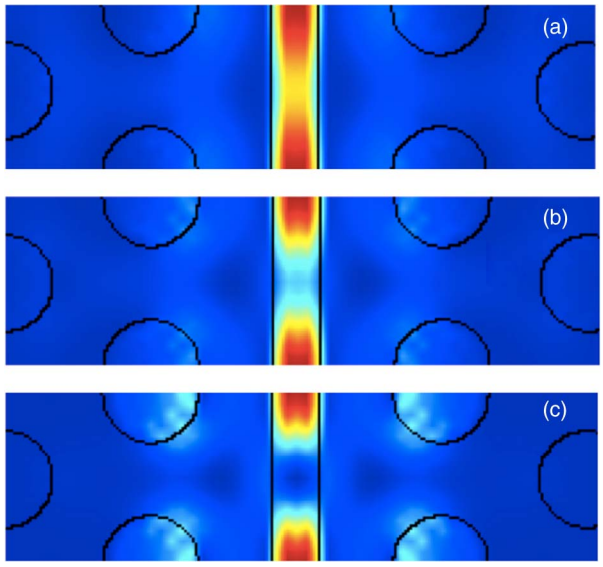

Fig. 4. Norm of the electric field ($|E|^2$) for a SPhC (slot width = 135 nm) at different group indices (ng = 3.6, 15, and 70 for panels (a), (b), and (c), respectively). In the fast-light regime (top), the field is concentrated inside the slot, and scattering from the slot sidewall dominates. As the group index increases (middle and bottom), the light spreads out and also samples the roughness on the first row of PhC holes, leading to additional propagation loss.

It is useful to remind here that each transmission curve is normalized to that of a set of uniform channel waveguides. Thus, a positive loss figure means that the SPhC waveguides would have a lower loss than a channel waveguide. The large error bar is due to the relatively short length of the waveguides, and in order to assess the losses more accurately, we need to evaluate longer waveguides, which is the subject of future work.

4. Discussion

From Fig. 3, we note two key features. First of all, the loss is dependent on the slot width, with narrower slots exhibiting higher losses. This can be explained by the tighter confinement of the field and the correspondingly increased light intensity on the slot sidewalls. Therefore, a higher proportion of the field is subjected to any roughness present on the walls. Conversely, for increasingly wider slots, the field is increasingly less confined in the low refractive index medium and penetrates into the patterned region, with a consequent increase in the loss figure. Second, propagation loss is strongly wavelength dependent. This is not surprising given the characteristic dispersion of PhC devices already discussed above. In addition, we note that the shape of the mode depends on its group velocity. Fig. 4 shows the norm of the electric field ($|E|^2$), for different wavelengths, corresponding to different speed, with group index ng equal to 3.6, 15, and 70, respectively. The simulations were performed with standard plane-wave analysis in three dimensions [24]. We increased the resolution of the numerical method until we did not notice any further change in the results. In the fast region of

the dispersion curve, away from the cutoff, light is mostly confined by the slot. At shorter wavelength, closer to the band edge, light starts to slow down and the field spreads out, sampling more of the PhC cladding. Therefore, in the fast regime, light scatters predominantly from the roughness on the slot sidewall, and we measure a loss figure comparable to that observed for a standard slot channel waveguide ($\simeq$10 dB/cm) [20]. Remarkably, this is also the same order of magnitude of that of a standard defect PhC waveguide [25]. This result appears somehow controversial, given that most of the field feels the slot interface. However, in the standard PhC case, and for comparable light speed (and confinement), the light samples the many interfaces of the first row of holes. Similarly, as one approaches the slow-light regime in slotted waveguides, the loss figure also worsens once the contribution of the slot adds to that of the holes.

5. Conclusion

We have measured the propagation losses of SPhC waveguides as a function of slot width. The results confirm that low loss propagation in SPhC devices is possible and that it is comparable to losses in non-SPhC waveguides or in slotted ridge waveguides. Therefore, propagation losses do not restrict the further exploration of high light–matter interaction in slotted waveguides, e.g., for sensing or nonlinear optics applications.

References

[1] A. Di Falco, L. O'Faolain, and T. F. Krauss, "Photonic crystal slotted slab waveguides," *Photon. Nanostruct.-Fundam. Appl.*, vol. 6, no. 1, pp. 38–41, 2008.

[2] A. Di Falco, L. O'Faolain, and T. F. Krauss, "Dispersion control and slow light in slotted photonic crystal waveguides," *Appl. Phys. Lett.*, vol. 92, no. 8, pp. 083501-1–083501-3, Feb. 2008.

[3] V. Almeida, Q. Xu, C. Barrios, and M. Lipson, "Guiding and confining light in void nanostructure," *Opt. Lett.*, vol. 29, no. 11, pp. 1209–1211, Jun. 2004.

[4] J. Joannopoulos, P. Villeneuve, and S. Fan, "Photonic crystals: Putting a new twist on light," *Nature*, vol. 386, no. 6621, pp. 143–149, Mar. 1997.

[5] T. F. Krauss, "Why do we need slow light?" *Nat. Photon.*, vol. 2, no. 8, pp. 448–450, Aug. 2008.

[6] B. Song, S. Noda, T. Asano, and Y. Akahane, "Ultra-high-Q photonic double-heterostructure nanocavity," *Nat. Mater.*, vol. 4, no. 3, pp. 207–210, Mar. 2005.

[7] E. Kuramochi, M. Notomi, S. Mitsugi, A. Shinya, T. Tanabe, and T. Watanabe, "Ultrahigh-Q photonic crystal nanocavities realized by the local width modulation of a line defect," *Appl. Phys. Lett.*, vol. 88, no. 4, pp. 041112-1–041112-3, Jan. 2006.

[8] A. Di Falco, C. Conti, and G. Assanto, "Quadratic phase matching in slot waveguides," *Opt. Lett.*, vol. 31, no. 21, pp. 3146–3148, Nov. 2006.

[9] C. A. Barrios, K. B. Gylfason, B. Sanchez, A. Griol, H. Sohlstroem, M. Holgado, and R. Casquel, "Slot-waveguide biochemical sensor," *Opt. Lett.*, vol. 32, no. 21, pp. 3080–3082, Nov. 2007.

[10] C. Koos, P. Vorreau, T. Vallaitis, P. Dumon, W. Bogaerts, R. Baets, B. Esembeson, I. Biaggio, T. Michinobu, F. Diederich, W. Freude, and J. Leuthold, "All-optical high-speed signal processing with silicon–organic hybrid slot waveguidesx," *Nat. Photon.*, vol. 3, no. 4, pp. 216–219, Apr. 2009.

[11] M. Hiscocks, C. Su, B. Gibson, A. Greentree, L. Hollenberg, and F. Ladouceur, "Slot-waveguide cavities for optical quantum information applications," *Opt. Exp.*, vol. 17, no. 9, pp. 7295–7303, Apr. 2009.

[12] A. Di Falco, L. O'Faolain, and T. F. Krauss, "Chemical sensing in slotted photonic crystal heterostructure cavities," *Appl. Phys. Lett.*, vol. 94, no. 6, pp. 063503-1–063503-3, Feb. 2009.

[13] J. Jagerska, H. Zhang, Z. Diao, N. Le Thomas, and R. Houdre, "Refractive index sensing with an air-slot photonic crystal nanocavity," *Opt. Lett.*, vol. 35, no. 15, pp. 2523–2525, Aug. 2010.

[14] M. G. Scullion, A. Di Falco, and T. F. Krauss, "Slotted photonic crystal cavities with integrated microfluidics for biosensing applications," *Biosens. Bioelectron.*, vol. 27, no. 1, pp. 101–105, Sep. 2011.

[15] J. H. Wülbern, J. Hampe, A. Petrov, M. Eich, J. Luo, A. K.-Y. Jen, A. Di Falco, T. F. Krauss, and J. Bruns, "Electro-optic modulation in slotted resonant photonic crystal heterostructures," *Appl. Phys. Lett.*, vol. 94, no. 24, pp. 241107-1–241107-3, Jun. 2009.

[16] X. Chen, Y.-S. Chen, Y. Zhao, W. Jiang, and R. T. Chen, "Capacitor-embedded 0.54 pJ/bit silicon-slot photonic crystal waveguide modulator," *Opt. Lett.*, vol. 34, no. 5, pp. 602–604, Mar. 2009.

[17] J. Brosi, C. Koos, L. C. Andreani, M. Waldow, J. Leuthold, and W. Freude, "High-speed low-voltage electro-optic modulator with a polymer-infiltrated silicon photonic crystal waveguide," *Opt. Exp.*, vol. 16, no. 6, pp. 4177–4191, Mar. 2008.

[18] X. Chen, W. Jiang, J. Chen, L. Gu, and R. T. Chen, "20 dB-enhanced coupling to slot photonic crystal waveguide using multimode interference coupler," *Appl. Phys. Lett.*, vol. 91, no. 9, pp. 091111-1–091111-3, Aug. 2007.

[19] M. G. Scullion, T. F. Krauss, and A. Di Falco, "High efficiency interface for coupling into slotted photonic crystal waveguides," *IEEE Photon. J.*, vol. 3, no. 2, pp. 203–208, Apr. 2011.

[20] T. Baehr-Jones, M. Hochberg, C. Walker, and A. Scherer, "High-Q optical resonators in silicon-on-insulator-based slot waveguides," *Appl. Phys. Lett.*, vol. 86, no. 8, pp. 081101-1–081101-3, Feb. 2005.
[21] T. Alasaarela, D. Korn, L. Alloatti, A. Saynatjoki, A. Tervonen, R. Palmer, J. Leuthold, W. Freude, and S. Honkanen, "Reduced propagation loss in silicon strip and slot waveguides coated by atomic layer deposition," *Opt. Exp.*, vol. 19, no. 12, pp. 11 529–11 538, Jun. 2011.
[22] A. Spott, T. Baehr-Jones, R. Ding, Y. Liu, R. Bojko, T. O'Malley, A. Pomerene, C. Hill, W. Reinhardt, and M. Hochberg, "Photolithographically fabricated low-loss asymmetric silicon slot waveguides," *Opt. Exp.*, vol. 19, no. 11, pp. 10 950–10 958, May 2011.
[23] L. O'Faolain, S. A. Schulz, D. M. Beggs, T. P. White, M. Spasenovic, L. Kuipers, F. Morichetti, A. Melloni, S. Mazoyer, J. P. Hugonin, P. Lalanne, and T. F. Krauss, "Loss engineered slow light waveguides," *Opt. Exp.*, vol. 18, no. 26, pp. 27 627–27 638, Dec. 2010.
[24] S. Johnson and J. Joannopoulos, "Block-iterative frequency-domain methods for Maxwell's equations in a planewave basis," *Opt. Exp.*, vol. 8, no. 3, pp. 173–190, Jan. 2001.
[25] M. Notomi, T. Tanabe, A. Shinya, E. Kuramochi, H. Taniyama, S. Mitsugi, and M. Morita, "Nonlinear and adiabatic control of high-Q photonic crystal nanocavities," *Opt. Exp.*, vol. 15, no. 26, pp. 17 458–17 481, Dec. 2007.